Stiffening of fluid membranes due to thermal undulations: Density-matrix renormalization-group study

Yoshihiro Nishiyama*
Department of Physics, Faculty of Science, Okayama University, Okayama 700-8530, Japan
(Received 2 September 2002; published 18 December 2002)

It has been considered that the effective bending rigidity of fluid membranes should be reduced by thermal undulations. However, recent thorough investigation by Pinnow and Helfrich revealed the significance of measure factors for the partition sum. Accepting the local curvature as a statistical measure, they found that fluid membranes are stiffened macroscopically. In order to examine this remarkable idea, we performed extensive *ab initio* simulations for a fluid membrane. We set up a transfer matrix that is diagonalized by means of the density-matrix renormalization group. Our method has an advantage, in that it allows us to survey various statistical measures. As a consequence, we found that the effective bending rigidity flows toward strong coupling under the choice of local curvature as a statistical measure. On the contrary, for other measures such as normal displacement and tilt angle, we found a clear tendency toward softening.

DOI: 10.1103/PhysRevE.66.061907 PACS number(s): 87.16.Dg, 87.16.Ac, 05.10.Cc

I. INTRODUCTION

Amphiphilic molecules in water segregate spontaneously into flexible extended surfaces called fluid (lipid) membranes [1,2]. The fluid membranes are free from both surface tension and shear modulus, and the elasticity is governed only by bending rigidity [3,4]. The Hamiltonian is given by the following form:

$$H=\int dA\left(\frac{\kappa}{2}J^2+\overline{\kappa}K\right). \tag{1}$$

The mean curvature J is given by the summation of two principal curvatures $J=c_1+c_2$, whereas the Gaussian curvature K is given by their product $K=c_1c_2$. The corresponding two moduli κ and $\overline{\kappa}$ are called the bending rigidity modulus and Gaussian-curvature modulus, respectively. The integration $\int dA$ extends over the whole membrane surface. Hereafter, we drop the Gaussian-modulus term ($\overline{\kappa}=0$), because this term is topologically invariant [1,2], and we restrict ourselves to a fixed topology (planar surface).

Contrary to its seemingly simple form, the Hamiltonian (1) brings about perplexing problems: As a matter of fact, under an actual representation with differential geometry [for instance, see Eq. (3) explained afterwards], it turns out that membrane's undulations are subjected to complicated mutual scatterings. Therefore, it is expected that the effective bending rigidity for macroscopic length scales differs from the bare rigidity owing to the thermally activated undulations. Aiming to clarify this issue, a number of renormalization-group analyses have been reported so far [5–7]. The results are summarized in the following renormalization-group equation,

$$\kappa'=\kappa-\alpha\frac{k_BT}{8\pi}\ln M, \tag{2}$$

with renormalized bending rigidity κ', temperature T, and the number of decimated molecules M. Literature agrees that the numerical prefactor in the above equation is $\alpha=3$. (A more detailed account of the historical overview would be found in Ref. [8].) Because of $\alpha>0$, the effective bending rigidity is reduced by thermally activated undulations. This conclusion might be convincing, because the membrane shape itself should be deformed by thermal undulations. As a matter of fact, it has been known that the orientational correlation is lost for long distances [9]. It is quite natural to

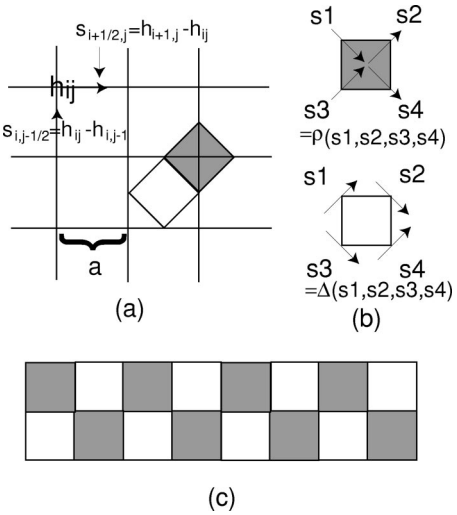

FIG. 1. (a) On the square lattice, we consider scalar field h_{ij} denoting normal displacement of a membrane with respect to a reference plane. Step variable (gradient field) $\vec{s}=a\vec{\partial}h$ is defined at each link. (b) The local statistical weights ρ [Eq. (7)] and Δ [Eq. (8)] are represented by shaded and open squares, respectively. The statistical weight ρ has several variants so as to take account of other integration measures such as curvature (11) and tilt angle (12). (c) From these local statistical weights, we construct a strip whose row-to-row statistical weight yields the transfer-matrix element. This transfer matrix is subjected to the DMRG diagonalization, as is shown in Fig. 2.

*Electronic address: nisiyama@psun.phys.okayama-u.ac.jp

anticipate that membranes become flexible for length scales exceeding this correlation length.

Recently, however, Pinnow and co-worker [8,10] obtained a remarkable conclusion $\alpha=-1(<0)$. The key ingredient of their new argument is that they considered the role of measure factors for the partition sum. They insist that the local mean curvature J should be the right statistical measure rather than other measures such as normal displacement $h(x,y)$ and local tilt angle $\theta(x,y)$. [The variable $h(x,y)$ denotes the normal displacement of the membrane from a base (reference) plane. We will explain it in the following section.] After an elaborated calculation of the variable replacement $h(x,y)\rightarrow J(x,y)$ and succeeding renormalization-group analysis, the authors reach the conclusion of $\alpha=-1$.

In order to examine their remarkable scenario, we performed first-principles simulation for a fluid membrane. Our simulation method has an advantage, in that we cover various integration measures in a unified way. In addition, our simulation does not rely on any perturbative treatments. Hence, it would be meaningful to complement the analytical perturbative treatment. We employed a transfer-matrix scheme, which is diagonalized by means of the density-matrix renormalization group [11–14]. It is to be noted that recently, such elastic (bosonic) systems came under thorough investigation by means of diagonalization after the advent of the density-matrix renormalization group [15–20].

It has to be mentioned that the Monte Carlo method has been utilized successfully in the studies of membranes and vesicles [1,2]. For the Monte Carlo method, however, a tethered (polymerized) membrane rather than a fluid membrane is more suitable [21], because a membrane is implemented in a computer as an assembly of molecules and junctions bearing close resemblance to a tethered membrane. However, Gompper and Kroll succeeded in simulating fluid membranes by the Monte Carlo method, allowing reconstructions of junctions during simulation (dynamical triangulation) [22]. They succeeded in observing the variation of the topological index with respect to the change of membrane concentration and temperature. In fairness, it has to be mentioned that their Monte Carlo data indicate softening for lipid vesicles.

The rest of this paper is organized as follows. In the following section, we explain our transfer-matrix formalism for a fluid membrane. We also explicate the density-matrix renormalization group with which we diagonalized the transfer matrix. In Sec. III, we calculate the effective bending rigidity. For that purpose, we introduce a scheme of coarse graining. Our data clearly support membrane stiffening under the choice of mean curvature $J(x,y)$ as a statistical measure. For other measures, on the contrary, we observed a tendency toward softening. In Sec. IV, we present summary and discussions.

II. TRANSFER-MATRIX FORMALISM AND ITS DIAGONALIZATION THROUGH THE DENSITY-MATRIX RENORMALIZATION GROUP

In this section, we present our numerical simulation technique. First, we explain our transfer-matrix formalism. Second, we introduce the density-matrix renormalization group with which we diagonalize the transfer matrix. A demonstration of the algorithm is also presented.

A. Transfer-matrix formalism

In order to describe the shape of membranes, it is convenient to use the Monge gauge [23]. In this frame, membrane deformation is described by a normal displacement (deformation) $h(x,y)$ from a base (reference) plane parametrized by Cartesian coordinates (x,y). In terms of this representation frame, the mean curvature $J(x,y)$ is given by

$$J(x,y)=\frac{(\partial_x^2 h+\partial_y^2 h)[1+(\partial_x h)^2+(\partial_y h)^2]-2\partial_x h\,\partial_y h\,\partial_x\partial_y h-\partial_x^2 h(\partial_x h)^2-\partial_y^2 h(\partial_y h)^2}{[1+(\partial_x h)^2+(\partial_y h)^2]^{3/2}} \tag{3}$$

explicitly. Similarly, the infinitesimal area dA is given by

$$dA=[1+(\partial_x h)^2+(\partial_y h)^2]^{1/2}\,dx\,dy. \tag{4}$$

Putting these together into the Hamiltonian (1), we obtain an explicit expression in terms of the displacement field $h(x,y)$.

Now, we are led to a two-dimensional scalar-field theory $h(x,y)$. However, the theory is afflicted by very complicated interactions. The aim of this paper is to investigate the theory beyond the perturbative level by means of an *ab initio* method. For that purpose, we put the theory on a square lattice with lattice constant a; see Fig. 1. Accordingly, the field variables $\{h_{ij}\}$ are now indexed by integer indices i and j. Throughout this paper, we set the lattice constant as the unit of length $a=1$. In other words, we are considering a square-netted membrane which was brought into thorough discussion in Ref. [10]. Readers may find convincing arguments why $J(x,y)$ is a physically sensible statistical measure. In particular, the authors think of a polymer chain, whose natural statistical measure is the angles between adjacent links. Likewise, for a fluid membrane, they found that the curvatures are the right statistical measure, continuing the polymer into a new space dimension to build up a membrane.

Our theory has the translational invariance of $h_{ij}\rightarrow h_{ij}+\Delta h$, and thus, the absolute value of h_{ij} should be meaningless. Therefore, we introduce the link variable

$$\vec{s} = a\vec{\partial}h \tag{5}$$

denoting the ''step'' at each link; see Fig. 1. Obviously, we are just performing the well-known duality transformation [24], which is very successful in the study of random surfaces. Note that now we arrive at a dual model with step variables $\{\vec{s}_{ij}\}$; see Fig. 1. For this dual model, the bending-energy cost exists at each plaquette, because it was originally a vertex possessing a curvature spanned by adjacent links. Hence, the statistical weight is associated with each plaquette,

$$\rho(s_1,s_2,s_3,s_4) = \exp\left[-a^2\sqrt{1+\left(\frac{s_1+s_4}{2a}\right)^2+\left(\frac{s_2+s_4}{2a}\right)^2}\,\frac{\kappa}{2}J(s_1,s_2,s_3,s_4)^2\right], \tag{6}$$

with

$$J(s_1,s_2,s_3,s_4) = -\frac{\left(\frac{s_4-s_1}{a^2}+\frac{s_2-s_3}{a^2}\right)\left[1+\left(\frac{s_1+s_4}{2a}\right)^2+\left(\frac{s_2+s_4}{2a}\right)^2\right]-\left(\frac{s_1+s_4}{2a}\right)^2\frac{s_4-s_1}{a^2}-\left(\frac{s_2+s_4}{2a}\right)^2\frac{s_2-s_3}{a^2}}{\left[1+\left(\frac{s_1+s_4}{2a}\right)^2+\left(\frac{s_2+s_4}{2a}\right)^2\right]^{1.5}}. \tag{7}$$

See also Fig. 1 for the notation of $\{s_\alpha\}$. We have set $k_BT=1$, because k_BT can be absorbed into the bending rigidity κ. It is apparent from the construction of the dual theory that the step variables are not fully independent. In the notation of Fig. 1, there exists a restriction of $s_1+s_2-s_3-s_4=0$ for each open plaquette. Therefore, we introduce the following statistical weight for each of them:

$$\Delta(s_1,s_2,s_3,s_4) = \delta_{s_1+s_2-s_3-s_4,0}. \tag{8}$$

As a consequence, we reach the lattice field theory with the statistical weights ρ, Eq. (7), and Δ, Eq. (8), which are arranged in the checkerboard pattern. Likewise, the transfer matrix is constructed as a striplike segment shown in Fig. 1. The transfer matrix is diagonalized by the density-matrix renormalization group.

In order to implement the above theory in a computer simulation, we must carry out yet another simplification. Namely, we discretize the link variable as follows:

$$s_i = \delta_s(i - N_s/2 - 0.5), \tag{9}$$

with $i=1,\ldots,N_s$. The unit of step, δ_s, is determined self-consistently through the simulation:

$$\delta_s = R\sqrt{\langle s_i^2\rangle}, \tag{10}$$

where $\langle\cdots\rangle$ denotes the thermal average. We made several trials for the tuning parameters of N_s and R; this discretization is the most influential factor concerning the reliability of our simulation. We will explore its reliability in the following section.

Our theory resembles the so-called solid-on-solid model, which exhibits the Kosterlitz-Thouless critical phase. Note that in our model, there is no surface-tension term, and there exists the bending elasticity κ instead. Therefore, our theory is not valid right at the critical phase, but it is rather driven off from it. The renormalization-group flow is actually the central concern of the present paper, and it is explored in the following section.

In the above, we did not pay any attention to the measure factor for the partition sum. As is emphasized in the Introduction, the measure factor should alter the underlying physics even qualitatively. As is apparent from the above formalism, particularly from Eq. (9), we accept uniform measure for the step variable, namely, we are accepting the normal displacement as the statistical measure. Following the idea advocated in Refs. [8,10], we will also consider the local mean curvature as for the statistical measure. The replacement of the integration variables is absorbed into the redefinition of the statistical weight. Namely, we made the replacement

$$\rho(s_1,s_2,s_3,s_4) \to \rho(s_1,s_2,s_3,s_4)\sqrt{\prod_{\alpha=1}^{4}\left|\frac{\partial J(s_1,s_2,s_3,s_4)}{\partial s_\alpha}\right|}. \tag{11}$$

The square root is intended to take the geometrical mean, because each step variable s_α is sheared by an adjacent plaquette as well.

In addition, we consider the local tilt angle as for the measure; namely, we made the replacement

$$\rho(s_1,s_2,s_3,s_4) \to \rho(s_1,s_2,s_3,s_4)\prod_{\alpha=1}^{4}\left|\cos\left(\arctan\frac{s_\alpha}{a}\right)\right|. \tag{12}$$

As a consequence, we have prepared three types of statistical weights, h [Eq. (7)], J [Eq. (11)], and θ [Eq. (12)], which are examined in the following section.

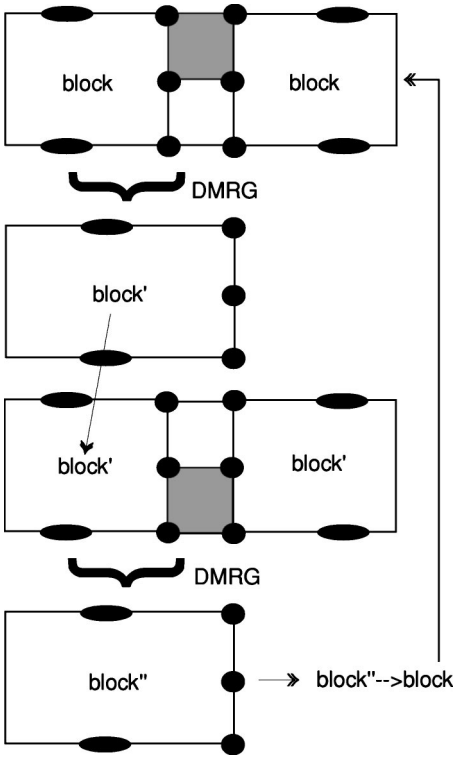

FIG. 2. Schematic drawing of the density-matrix normalization group (DMRG) procedure [11–14]. From the drawing, we see that through DMRG, a ''block'' and the adjacent site are renormalized into a new ''block′;'' similarly, block′→block″. At this time, the number of block states is retained within *m*; see text. In this manner, we can diagonalize a large-scale transfer matrix through successive application of DMRG. A demonstration of the algorithm is presented in Figs. 3 and 4.

B. Diagonalization of the transfer matrix with density-matrix renormalization group

In the preceding section, we have set up the transfer matrix. In principle, one would extract various informations if one could diagonalize the transfer matrix. However, in practice, the matrix size exceeds the limit of computer-memory size. Such difficulty arises in common with such systems called soft matters, which exhibit, by nature, vast numbers of vibration modes. Therefore, the Monte Carlo technique has been employed in order to simulate soft matters. However, after the advent of the density-matrix renormalization group [11–13], the difficulty was removed, and now, soft matters (elastic systems) have come under thorough investigation by means of the diagonalization method; examples are lattice vibrations [15,16], collection of oscillators as a heat bath [17], string meandering motions [18,19], and lattice scalar-field theory [20]. In essence, the technique allows us to discard ''irrelevant states,'' and hence, the number of states are truncated so as to save the computer-memory space.

Below, we will explain the density-matrix renormalization group. Our algorithm is standard, and a pedagogical guide can be found in Ref. [13] as well. The transfer matrix is represented by a strip shown in Fig. 1. Our goal is to diagonalize the transfer matrix with sufficient length. We will show that this goal is achieved by the recursive application

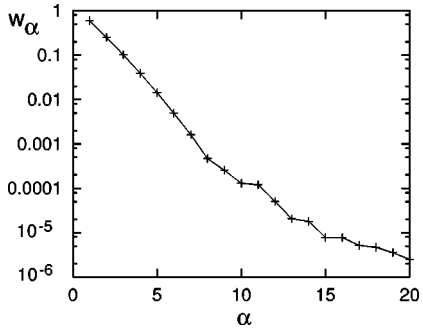

FIG. 3. Distribution of the eigenvalues (weights) $\{w_\alpha\}$ (α, integer index) of the density matrix for bending rigidity $\kappa=0.5$. Simulation parameters are $m=13$, $N_s=9$, and $R=0.9$; see Eq. (9). We see that w_α vanishes very rapidly for large α. In the simulation, we retained relevant states up to $m=13$, and we achieved a precision of $\sim 10^{-5}$. In this manner, the number of states of the ''block'' in Fig. 2 is truncated (renormalized).

of the density-matrix renormalization group. The renormalization procedures are presented in Fig. 2, where two sets of renormalizations are shown. Through each renormalization, a ''block'' and the adjacent site are renormalized into a new ''block′;'' and similarly, block′→block″. The crucial point is that the number of states for a block is kept within *m*. Therefore, we can iterate the procedure until the strip becomes sufficiently long. Such truncation of block states within *m* is managed in the following manner [11,12]: One first constructs the density matrix $\rho_{B+\bullet}$ [11–14] with respect to the part of system composed of the block and the adjacent site. Then, ''relevant states'' are extracted from the eigenstates $\{u_\alpha\}$ of the density matrix with relatively larger eigenvalues $\{w_\alpha\}$; the density-matrix eigenvalues $\{w_\alpha\}$ are called ''weights.'' Because the weight w_α becomes almost negligible for large α, we just retain relevant *m* states with dominant weight, and discard the other remaining states. In this manner, the block and the site are renormalized into a new block, whose states are represented by the truncated bases $\{u_\alpha\}$ with $\alpha=1,\ldots,m$.

Let us demonstrate the reliability. We will accept the local curvature as the statistical measure. In Fig. 3, we present the distribution of weight $\{w_\alpha\}$ after 40 renormalizations for

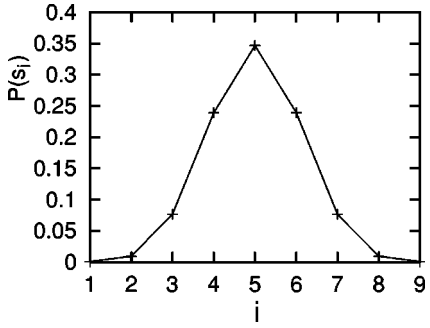

FIG. 4. Probability distribution of the step variable $P(s_i)$; see Eq. (9), where we had set the threshold for the range of step variables as $\{s_i\}$ ($i=1,\ldots,N_s$). The simulation parameters are the same as those of Fig. 3. The range of step variables seems to cover the actual fluctuation deviation.

bending rigidity $\kappa=0.5$. Simulation parameters are set to be $m=13$, $N_s=9$, and $R=0.9$; see Eq. (9) for details. We see that the weight vanishes very rapidly. In the simulation, we retain $m=13$ weighted states, and we attain the precision of $\sim 10^{-5}$. In Fig. 4, we present the probability distribution of the step variable. Because we have bounded the range of step variable as in Eq. (9), we must check whether it covers the actual thermal fluctuation deviation. The range of step variables seems to cover the actual fluctuation deviation. Hence, our treatment of Eq. (9) turns out to be justified. In all simulations presented hereafter, we had monitored such a performance check carefully.

III. REAL-SPACE DECIMATION AND EFFECTIVE BENDING RIGIDITY: APPLICATION OF THE DENSITY-MATRIX RENORMALIZATION GROUP

In this section, we study the effective bending rigidity of a fluid membrane. For that purpose, we introduce a scheme of real-space decimation [25]. Then, we apply the density-matrix renormalization group. All data are calculated after 40 renormalizations; namely, the length of the transfer matrix extends to $L=80$.

To avoid confusion, note the following: In this paper, the word ''renormalization'' is used in two different contexts. First, we employ the density-matrix *renormalization* group as a simulation technique. Secondly, we manage the real-space *renormalization* to get information on effective bending rigidity. The former terminology is named after the fact that we *renormalize* irrelevant states in order to save computer-memory size. The latter is aimed to gain the *renormalization*-group flow with the length scale changed.

A. Real-space decimation

Real-space decimation (coarse graining) was first introduced in the study of critical phenomena [26]; in particular, it was aimed to interpret the scaling hypothesis. Later on, the idea was extended to meet more practical purposes such as the quantitative estimation of critical exponents and flow equations [27]. We follow Swendsen's version of real-space decimation, which has been proven to be very successful [25].

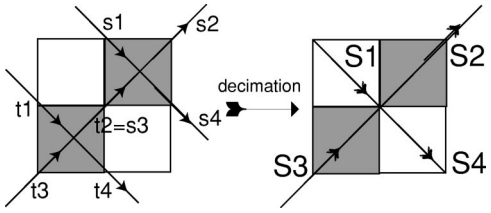

FIG. 5. Real-space decimation procedure. From the decimation, a new coarse-grained curvature $\tilde{J}$, Eq. (14), is constructed. $\tilde{J}$ is used in the succeeding renormalization-group analysis; see Fig. 6.

In Fig. 5, we have presented the real-space-decimation procedure. Note that two unit cells are renormalized into one enlarged unit cell. In other words, two molecules are renormalized into a new molecule, and hence, the parameter M in Eq. (2) is $M=2$. Correspondingly, from microscopic step variables $\{s_\alpha\}$ and $\{t_\alpha\}$, we construct the coarse-grained step variables

$$S_1=(s_1+t_1)/2,$$

$$S_2=s_3/2+s_2,$$

$$S_3=s_3/2+t_3,$$

$$S_4=(s_4+t_4)/2. \tag{13}$$

For this coarse-grained length scale, the curvature is given by

$$\tilde{J}=-\frac{\left(\frac{S_4-S_1}{(1.5a)^2}+\frac{S_2-S_3}{(1.5a)^2}\right)\left[1+\left(\frac{S_1+S_4}{3a}\right)^2+\left(\frac{S_2+S_4}{3a}\right)^2\right]-\left(\frac{S_1+S_4}{3a}\right)^2\frac{S_4-S_1}{(1.5a)^2}-\left(\frac{S_2+S_4}{3a}\right)^2\frac{S_2-S_3}{(1.5a)^2}}{\left[1+\left(\frac{S_1+S_4}{3a}\right)^2+\left(\frac{S_2+S_4}{3a}\right)^2\right]^{1.5}}. \tag{14}$$

After coarse graining, one must redefine the unit of length accordingly; namely,

$$a\to a/\sqrt{2},$$

$$h_{ij}\to h_{ij}/\sqrt{2}. \tag{15}$$

The coarse-grained membrane may be described by the Hamiltonian $H=\int dA\kappa'\tilde{J}^2/2$ with a renormalized bending rigidity κ'. As is well known, the transformation coefficient $\partial\kappa'/\partial\kappa$ contains much information on the infrared behavior of the effective coupling constant [25]. Anticipated behaviors of κ-κ' are drawn schematically in Fig. 6. From the figure, we see that for $\partial\kappa'/\partial\kappa>1$, the membrane is stiffened in the infrared limit, whereas for $\partial\kappa'/\partial\kappa>1$, the membrane is softened. The transformation coefficient $\partial\kappa'/\partial\kappa$ is given by the chain relation [25]

$$\frac{\partial\langle\tilde{J}^2dA\rangle}{\partial\kappa}=\frac{\partial\kappa'}{\partial\kappa}\frac{\partial\langle\tilde{J}^2dA\rangle}{\partial\kappa'}. \tag{16}$$

Here, dA denotes the area of the membrane segment shown in Fig. 5. The remaining task is to perform the above numeri-

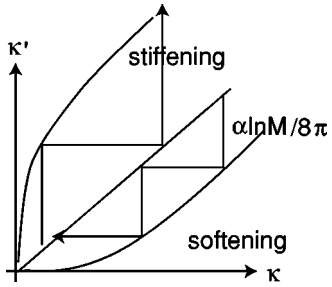

FIG. 6. Schematic flow diagram of the effective bending rigidity $\kappa \to \kappa'$. Depending on the transformation coefficient $\partial\kappa'/\partial\kappa > 1$ (<1), the membrane is stiffened (softened) in the infrared limit.

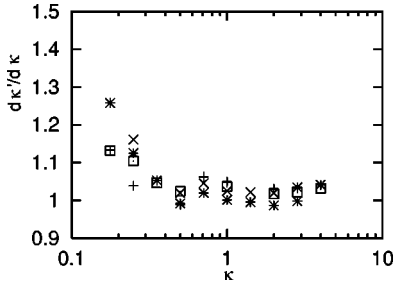

FIG. 7. Transformation coefficient $\partial\kappa'/\partial\kappa$ is plotted for bare rigidity κ. We have accepted the local curvature as for the statistical measure. The simulation parameters for each symbol are $(+)$ $m=12$, $N_s=7$, and $R=0.9$; $(\times)$ $m=12$, $N_s=7$, and $R=1.1$; $(*)$ $m=11$, $N_s=8$, and $R=0.9$; and $(\square)$ $m=15$, $N_s=6$, and $R=1.1$; see Eq. (9) for details. Referring to the anticipated behavior shown in Fig. 6, we see that the membrane is stiffened effectively in the infrared limit.

cal derivatives. Numerical differentiations are possible, because our data are free from statistical errors. That is a great advantage of our algorithm over others such as Monte Carlo. We adopted Richardson's deferred approach to the limit algorithm in the text book [28]. In this algorithm, one makes an extrapolation after calculating various finite-difference differentiations. We monitored the relative error, and checked that the error is kept within 10^{-3}.

B. Membrane stiffening in the case of local-curvature measure

Following the idea of Refs. [8,10], we will accept the local curvature $J(x,y)$ as for the statistical measure. This is achieved by adopting the statistical weight (11) in the construction of the transfer matrix. In Fig. 7, we plotted the transformation coefficient $\partial\kappa'/\partial\kappa$, Eq. (16), for the bare coupling $0.17<\kappa<4$. In obtaining the data, we have made a number of trials for the simulation parameters of m (number of block states), N_s, and R (range of step variables); see Eq. (9) for details. Thereby, we confirm that good convergence is achieved with respect to the tuning parameters.

From Fig. 7, we see that the inequality $\partial\kappa'/\partial\kappa > 1$ holds. Referring to the anticipated behavior depicted in Fig. 6, we found that the membrane is stiffened effectively for macroscopic length scales. As a matter of fact, for other integration measures, the inequality $\partial\kappa'/\partial\kappa > 1$ is not satisfied, as will be shown in the following section. Our simulation result is the first *ab initio* support of the analytical argument by Pinnow and co-worker [8,10].

In the figure, for small rigidity $\kappa<1$, where thermal undulations should be enhanced, we observe a notable enhancement of the transformation coefficient $\partial\kappa'/\partial\kappa$. Hence, it is indicated that this stiffening is driven, quite contrary to our naive expectation, by thermal undulations. This rather counterintuitive result suggests that the ''hat excitation'' [8], which is a sort of solitonic excitation, would be created over the membrane surface: The hat excitation is a solitonic object accompanying localized dimplelike deformation. In Ref. [8], the author claimed that the hat excitations cause, unlike conventional sinusoidal undulations, membrane stiffening. It would be astonishing that for such small rigidity $\kappa<0.5$, where the membrane should be crumpled considerably, the concept of hat excitation is still applicable. This fact may tell that the hat excitation is indeed solitonic in the sense that hat excitations are stable under collisions, and the thermal undulations can be decomposed into individually propagating hat excitations.

It is to be noted that such pronounced enhancement of $\partial\kappa'/\partial\kappa$ for small κ is not captured by the analytical one-loop renormalization-group treatment (2), because it just yields $\partial\kappa'/\partial\kappa=1$ for all κ. (It might be convincing, because analytical perturbative treatment should be justified for sufficiently rigid membranes.) This is obviously the advantage of our first-principles simulation. For exceedingly small rigidity $\kappa<0.17$, however, the membrane becomes too crumpled, and we cannot continue reliable simulation. (From a technical viewpoint, the density-matrix weight exhibits almost uniform distribution, and we cannot set any reasonable threshold for the truncation of states.)

On the other hand, for the large-rigidity side $\kappa>1$, we see that the transformation coefficient approaches the neutral value $\partial\kappa'/\partial\kappa \approx 1$. Note that the analytical one-loop renormalization-group analysis (2) yields $\partial\kappa'/\partial\kappa=1$. Hence, we see that for sufficiently large κ, the analytical result (2) is recovered asymptotically.

C. Membrane softening under the statistical measures of $h(x,y)$ and $\theta(x,y)$

For other integration measures such as normal displacement $h(x,y)$, Eq. (7), and tilt angle $\theta(x,y)$, Eq. (12), we found behaviors quite contrasting to that shown in the preceding subsection. In Fig. 8, we plotted the transformation coefficient $\partial\kappa'/\partial\kappa$ for the normal-displacement integration measure (7). (Note that this integration measure has been widely used so far in the analytical calculations except Refs. [8,10].) From the figure, we see that $\partial\kappa'/\partial\kappa<1$ definitely holds. Hence, in this case, the membrane is softened effectively for macroscopic length scales; see the schematic behavior shown in Fig. 6. In addition, it is to be noted that for small rigidity $\kappa<1$, the transformation coefficient $\partial\kappa'/\partial\kappa$ is suppressed, and it approaches the neutral value $\partial\kappa'/\partial\kappa=1$ as the membrane rigidity κ increases. This fact tells that the softening is driven by the thermal undulations. Note that the

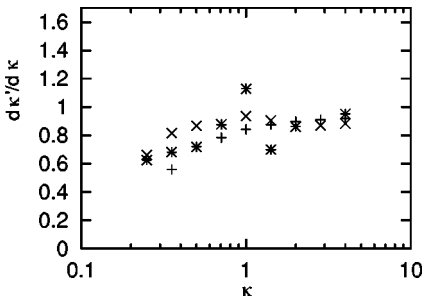

FIG. 8. Transformation coefficient $\partial\kappa'/\partial\kappa$ is plotted for bare rigidity κ. We have accepted the normal displacement as for the statistical measure. The simulation parameters for each symbol are $(+)$ $m=12$, $N_s=7$, and $R=0.8$; $(\times)$ $m=10$, $N_s=9$, and $R=0.6$; and $(*)$ $m=11$, $N_s=8$, and $R=0.7$; see Eq. (9) for details. Referring to the anticipated behavior shown in Fig. 6, we see that the membrane is softened effectively in the infrared limit.

effect of thermal undulations appears in a way quite opposite to the aforementioned $J(x,y)$ statistical measure.

In the case of the tilt-angle statistical measure (12), the transformation coefficient exhibits similar behavior $\partial\kappa'/\partial\kappa<1$; see Fig. 9. However, $\partial\kappa'/\partial\kappa$ is much closer to the neutral value $\partial\kappa'/\partial\kappa\approx 1$, suggesting that the extent of softening is smaller than that of the normal-displacement integration measure. In other words, the membrane shape would stay almost scale invariant under the choice of tilt angle as for the statistical measure.

In the calculations presented in this section [particularly, for the $h(x,y)$ measure], the simulations suffered from instabilities coming from unbounded undulations due to membrane softening. More specifically, during the simulation, the membrane becomes crumpled spontaneously, and the membrane shape is trapped in a certain metastable configuration. Such pathology may arise because there are exceedingly numerous thermally activated configurations of almost equal statistical weight. Diagonalization of the transfer matrix thus fails in searching for the true globally stable thermal equilibrium. Moreover, the postulation of Eq. (9) has not been fully justified, where we had assumed that the range of the step variable is bounded. As the simulation parameters of m and N_s are improved, these instabilities are avoided to some extent. In a sense, these instabilities reflect the fact that the membrane is softened indeed, and the shape fluctuations are enhanced for long distances. From the above experience, we are led to the speculation that the Monge gauge would not be very justified for the description of fluid membranes in the case of softening, at least, beyond perturbative level.

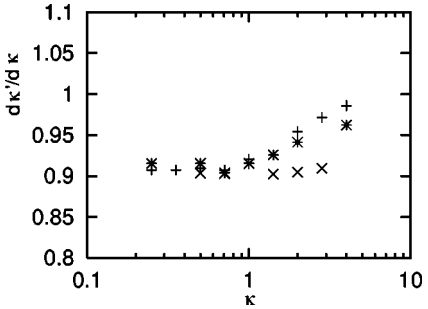

FIG. 9. Transformation coefficient $\partial\kappa'/\partial\kappa$ is plotted for bare rigidity κ. We have accepted the local tilt angle as for the statistical measure. The simulation parameters for each symbol are $(+)$ $m=10$, $N_s=9$, and $R=0.7$; $(\times)$ $m=12$, $N_s=7$, and $R=0.7$; and $(*)$ $m=11$, $N_s=8$, and $R=0.7$; see Eq. (9) for details. Referring to the anticipated behavior shown in Fig. 6, we see that the membrane is softened effectively in the infrared limit.

IV. SUMMARY AND DISCUSSIONS

We have investigated the effective bending rigidity (2) of a fluid membrane (1) for macroscopic length scales. The effective rigidity has been arousing renewed interest, since Pinnow and Helfrich pointed out that the membranes would be *stiffened* by thermal undulations. The key ingredient of their argument is that the local curvature should be the right statistical measure for the partition sum. Motivated by this remarkable scenario, we had performed first-principles simulation with the transfer-matrix method and the density-matrix renormalization group; see Figs. 1 and 2. Our simulation scheme does not rely on any perturbative treatments, and it covers various statistical measures such as local curvature (11), normal displacement (7), and tilt angle (12). Because analytical variable replacements among these variables require rather tedious task even on the perturbative level, it would be meaningful to survey various measure factors systematically by *ab initio* simulation. The performance of the simulation scheme is demonstrated in Figs. 3 and 4.

We introduced a scheme of real-space decimation as is shown in Fig. 5, and correspondingly, we defined coarse-grained curvature $\tilde{J}$, Eq. (14). These preparations enable us to calculate the transformation coefficient $\partial\kappa'/\partial\kappa$, Eq. (16), from which we read off the direction of the renormalization-group flow; its anticipated behaviors are drawn schematically in Fig. 6. As a consequence, using the statistical measures, we observed clear distinction between the mean curvature $\partial\kappa'/\partial\kappa>1$ and the others $\partial\kappa'/\partial\kappa<1$. Namely, when we accept mean curvature as a statistical measure, the effective rigidity is, in fact, renormalized toward strong coupling; see Fig. 7. That is, membrane stiffening takes place. On the contrary, both normal displacement and tilt angle appear to lead to membrane softening; see Figs. 8 and 9. Our simulation results are an *ab initio* support of the aforementioned analytical argument [8].

Apart from mere curiousity, the membrane stiffening is quite favorable for the consistency of our numerical simulation: In our simulation, in the first place, we had restricted the range of step variables as in Eq. (16). Apparently, this postulation is in favor of membrane stiffening. In addition, we had discarded irrelevant states through the density-matrix renormalization group in order to keep the number of states tractable in computers. Again, this truncation of states is validated consequently after the onset of membrane stiffening. Furthermore, we believe that the very starting point of our theory, namely, the Monge gauge, is in favor of membrane stiffening, because it is assumed that there exists a reference plane from which all undulations are excited. Membrane stiffening may serve solid grounds for the Monge gauge.

For those reasons, we could perform well-controlled simulation in the case of membrane stiffening. On the contrary, as for the case of membrane softening, our simulation faces a number of conflicts coming from unbounded undulations as the strip length of the transfer matrix is enlarged; see Sec. III C for details. Because such pronounced undulations lack the grounds of the reference plane, it would be rather unwise to adopt the Monge gauge at least beyond perturbative level. By the way, we are fairly confident of the efficiency of our simulation in the case of membrane stiffening, and we believe that membrane stiffening may serve as a new promising research field for the application of the density-matrix renormalization group.

The following problems remain open: First, in Ref. [8], the author pointed out an intriguing picture of the deformation mode called ''hat excitation.'' This is a sort of soliton that is in contrast to the naive sinusoidal undulation. With the hat-excitation picture, the author provided valuable physical insights. First-principles examination of the reality of this hat excitation would be desirable. Second, irrespective of the membrane stiffening, the correlation length is known to be finite, and the orientational correlation is lost for long distances [9]. In Ref. [8], it is speculated that the two modes, namely, orientation and curvature, would be decoupled. A deeper understanding of the above points would establish the justification that the local curvature is the right statistical measure.

ACKNOWLEDGMENT

This work was supported by a Grant-in-Aid for Young Scientists (No. 13740240) from Monbusho, Japan.

[1] R. Lipowsky, Nature (London) **349**, 475 (1991).
[2] L. Peliti, in *Fluctuating Geometries in Statistical Mechanics and Field Theory*, edited by F. David, P. Ginsparg, and J. Zinn-Justin (Elsevier Science, Amsterdam, 1996).
[3] P. Canham, J. Theor. Biol. **26**, 61 (1970).
[4] W. Helfrich, Z. Naturforsch. C **28**, 693 (1973).
[5] L. Peliti and S. Leibler, Phys. Rev. Lett. **54**, 1690 (1985).
[6] D. Förster, Phys. Lett. **114A**, 115 (1986).
[7] H. Kleinert, Phys. Lett. **114A**, 263 (1986).
[8] W. Helfrich, Eur. Phys. J. B **1**, 481 (1998).
[9] P.G. de Gennes and C. Taupin, J. Phys. Chem. **86**, 2294 (1982).
[10] H.A. Pinnow and W. Helfrich, Eur. Phys. J. E **3**, 149 (2000).
[11] S.R. White, Phys. Rev. Lett. **69**, 2863 (1992).
[12] S.R. White, Phys. Rev. B **48**, 10 345 (1993).
[13] *Density-Matrix Renormalization: A New Numerical Method in Physics*, edited by I. Peschel, X. Wang, M. Kaulke, and K. Hallberg (Springer-Verlag, Berlin, 1999).
[14] T. Nishino, J. Phys. Soc. Jpn. **64**, 3598 (1995).
[15] L.G. Caron and S. Moukouri, Phys. Rev. Lett. **76**, 4050 (1996).
[16] C. Zhang, E. Jeckelmann, and S.R. White, Phys. Rev. Lett. **80**, 2661 (1998).
[17] Y. Nishiyama, Eur. Phys. J. B **12**, 547 (1999).
[18] Y. Nishiyama, Phys. Rev. B **64**, 064510 (2001).
[19] Y. Nishiyama, Phys. Rev. B **66**, 184501 (2002).
[20] Y. Nishiyama, J. Phys. A **34**, 11215 (2001).
[21] Y. Kantor, M. Kardar, and D.R. Nelson, Phys. Rev. Lett. **57**, 791 (1986).
[22] G. Gompper and D.M. Kroll, J. Phys.: Condens. Matter **12**, A29 (2000).
[23] P.M. Chaikin and T.C. Lubensky, *Principles of Condensed Matter Physics* (Cambridge University Press, Cambridge, 1995).
[24] J. Villain, J. Phys. (Paris) **36**, 581 (1975).
[25] R.H. Swendsen, in *Real-Space Renormalization*, edited by T. W. Burkhardt and J.M.J. van Leeuwen (Springer-Verlag, Berlin, 1982).
[26] L.P. Kadanoff, W. Götze, D. Hamblen, R. Hecht, E.A.S. Lewis, V.V. Palciauskas, M. Rayl, J. Swift, D. Aspnes, and J. Kane, Rev. Mod. Phys. **39**, 395 (1967).
[27] S.-K. Ma, Phys. Rev. Lett. **37**, 461 (1976).
[28] W.H. Press, S.A. Teukolsky, W.T. Vetterling, and B.P. Flannery, *Numerical Recipes in FORTRAN* (Cambridge University Press, Cambridge, 1992).